Thermal transport and irreversibility in rotating MHD hybrid nanofluid flow under the Cattaneo–Christov heat flux model

Abstract

The present study investigates the combined effects of thermal relaxation and magnetic field on the transport characteristics of an electrically conducting fluid using the modified Fourier law, namely the Cattaneo–Christov heat-flux model. Unlike the classical Fourier formulation, the proposed model accounts for finite thermal propagation speed and eliminates the paradox of instantaneous heat transfer. The governing nonlinear partial differential equations describing the momentum and energy transport are transformed into a coupled system of nonlinear ordinary differential equations through appropriate similarity transformations. The resulting boundary value problem is solved numerically using the `bvp5c` scheme. A detailed parametric analysis is performed to examine the influence of the magnetic parameter, Prandtl number, Eckert number, thermal stratification parameter, material parameter, and thermal relaxation parameter on the velocity, temperature, and microrotation profiles. The results reveal that an increase in the thermal relaxation parameter significantly suppresses the temperature distribution and reduces the local Nusselt number, indicating delayed thermal response within the fluid. Furthermore, the magnetic field is found to decelerate the fluid motion due to the Lorentz force, while enhancing thermal energy accumulation. A comparative analysis between the classical Fourier and Cattaneo–Christov heat-flux models highlights notable deviations in thermal behavior, particularly at higher relaxation times. The numerical results are validated through comparison with existing literature for limiting cases, demonstrating excellent agreement. The present findings provide deeper physical insight into non-Fourier heat transport mechanisms and are relevant to advanced thermal systems involving high-frequency heating, micro–nano scale transport, and energy conversion devices.

Keywords: Cattaneo–Christov heat flux; Non-Fourier heat conduction; Magnetohydrodynamics; Thermal relaxation; Boundary layer flow; Heat transfer enhancement; Numerical analysis

I. INTRODUCTION

Heat transfer processes are fundamental to a wide range of engineering and industrial systems, including thermal management of electronic devices, energy conversion technologies, nuclear reactors, geothermal applications, and micro–nano scale thermal transport. The ability to accurately model and predict thermal transport mechanisms is essential for the efficient design and optimization of modern thermal systems. As technological devices become smaller and operate under more extreme thermal conditions, classical heat transfer models often require modification in order to capture the underlying physical phenomena more accurately.

In the classical theory of heat conduction, Fourier's law is commonly used to describe the relationship between heat flux and temperature gradient. Although this formulation has been successfully applied to many conventional heat transfer problems, it predicts instantaneous propagation of thermal disturbances throughout the medium. Such an assumption leads to an unrealistic prediction of infinite thermal wave speed. In many modern engineering applications involving high-frequency heating, micro-scale thermal transport, and ultra-fast thermal processes, the assumption of instantaneous heat propagation is not physically realistic. Consequently, more advanced thermal models that account for finite heat propagation speed have received increasing attention.

The incorporation of thermal relaxation effects into heat conduction models provides a more realistic representation of energy transport in such systems. By introducing a thermal relaxation time into the heat flux formulation, the propagation of thermal disturbances occurs with a finite speed, which resolves the paradox associated with classical Fourier heat conduction. This modification becomes particularly important in materials with complex microstructures, nano-scale thermal systems, and high-speed thermal processes where delayed thermal response significantly influences temperature distributions and heat transfer rates.

Another major development in modern heat transfer research is the introduction of nanofluids. Nanofluids are engineered suspensions of nano-sized solid particles dispersed within conventional base fluids. The presence of nanoparticles substantially enhances the thermal conductivity and energy transport capability of the fluid. Because of their superior thermophysical properties, nanofluids have attracted considerable attention for

improving the efficiency of heat transfer devices such as heat exchangers, solar collectors, cooling systems, and energy storage units. The interaction between nanoparticles and the base fluid modifies both momentum and thermal boundary layer structures, leading to complex flow and heat transfer characteristics.

In many practical applications, fluid flow occurs in the presence of magnetic fields, particularly when the working fluid is electrically conducting. Magnetohydrodynamic (MHD) effects arise when electromagnetic forces interact with the motion of the fluid, altering the velocity distribution and thermal transport behavior. The application of magnetic fields can significantly influence the flow structure, suppress fluid motion, and modify the thermal boundary layer thickness through the action of the Lorentz force. MHD flows are widely encountered in metallurgical processes, electromagnetic pumps, plasma physics, liquid metal cooling systems, and advanced energy technologies.

Rotational motion and stretching surfaces are also important features in many engineering systems, including rotating machinery, turbomachinery, polymer extrusion processes, and material manufacturing techniques. The presence of rotation introduces additional inertial forces that alter the fluid dynamics and heat transfer characteristics. The combined effects of rotation, magnetic fields, viscous dissipation, and enhanced thermal conductivity due to nanoparticles lead to highly nonlinear transport phenomena that require detailed mathematical modeling and numerical analysis.

Motivated by these considerations, the present study investigates the thermal transport characteristics of a rotating magnetohydrodynamic hybrid nanofluid flow incorporating finite-speed heat conduction effects. The mathematical formulation accounts for the combined influence of magnetic fields, rotational motion, viscous dissipation, and thermal relaxation. The governing nonlinear partial differential equations representing conservation of mass, momentum, and energy are transformed into a system of coupled nonlinear ordinary differential equations through appropriate similarity transformations.

The resulting boundary value problem is solved numerically, and the influence of key dimensionless parameters on velocity profiles, temperature distribution, heat transfer rate, and entropy generation is analyzed in detail. Particular attention is given to understanding how thermal relaxation modifies heat transport mechanisms in magnetohydrodynamic rotating nanofluid systems. The outcomes of this investigation provide deeper physical insight into non-Fourier heat transfer behavior and may contribute to the development of advanced thermal technologies involving enhanced heat transfer fluids and high-performance energy systems.

Despite the extensive studies on nanofluid heat transfer and magnetohydrodynamic flows, limited investigations have considered the combined effects of rotation, hybrid nanoparticles, and finite-speed heat conduction under the Cattaneo–Christov heat flux framework. Furthermore, entropy generation analysis for such systems remains insufficiently explored. Therefore, the present study aims to investigate the thermal transport and irreversibility characteristics of rotating MHD hybrid nanofluid flow incorporating the Cattaneo–Christov heat flux model.

NOMENCLATURE

M	Magnetic parameter
λ	Rotation parameter
Pr	Prandtl number
Ec	Eckert number
γ	Thermal relaxation parameter
ϕ	Nanoparticle volume fraction
Re_x	Local Reynolds number
Nu_x	Local Nusselt number
Be	Bejan number
Ns	Entropy generation number
u, v, w	Velocity components in x, y, z directions
T	Fluid temperature
q	Heat flux vector

II. MATHEMATICAL FORMULATION AND GOVERNING EQUATIONS

We consider a steady, incompressible, electrically conducting hybrid nanofluid flow over a stretching surface in a rotating frame. Heat transfer is modeled using the Cattaneo–Christov heat-flux theory.

A. Cattaneo–Christov heat flux

$$\mathbf{q} + \lambda_t \left[\frac{D\mathbf{q}}{Dt} - (\nabla \mathbf{V})\mathbf{q} - \mathbf{q}(\nabla \mathbf{V})^T \right] = -k\nabla T, \tag{1}$$

where $\mathbf{q}$ is the heat-flux vector, λ_t is the thermal relaxation time, $\mathbf{V} = (u, v, w)$ is the velocity vector, and k is the thermal conductivity.

B. Governing equations

$$\frac{\partial u}{\partial x} + \frac{\partial v}{\partial y} = 0. \tag{2}$$

$$u\frac{\partial u}{\partial x} + v\frac{\partial u}{\partial y} - 2\Omega w = \nu_{hnf}\frac{\partial^2 u}{\partial y^2} - \frac{\sigma_{hnf} B_0^2}{\rho_{hnf}} u. \tag{3}$$

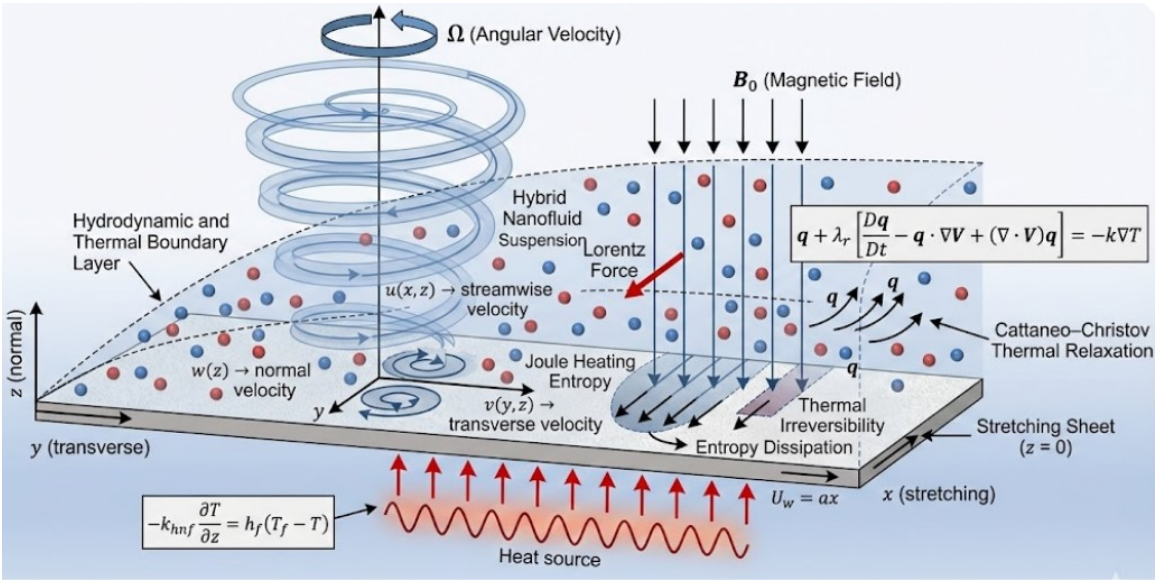

FIG. 1: Geometry of the problem.

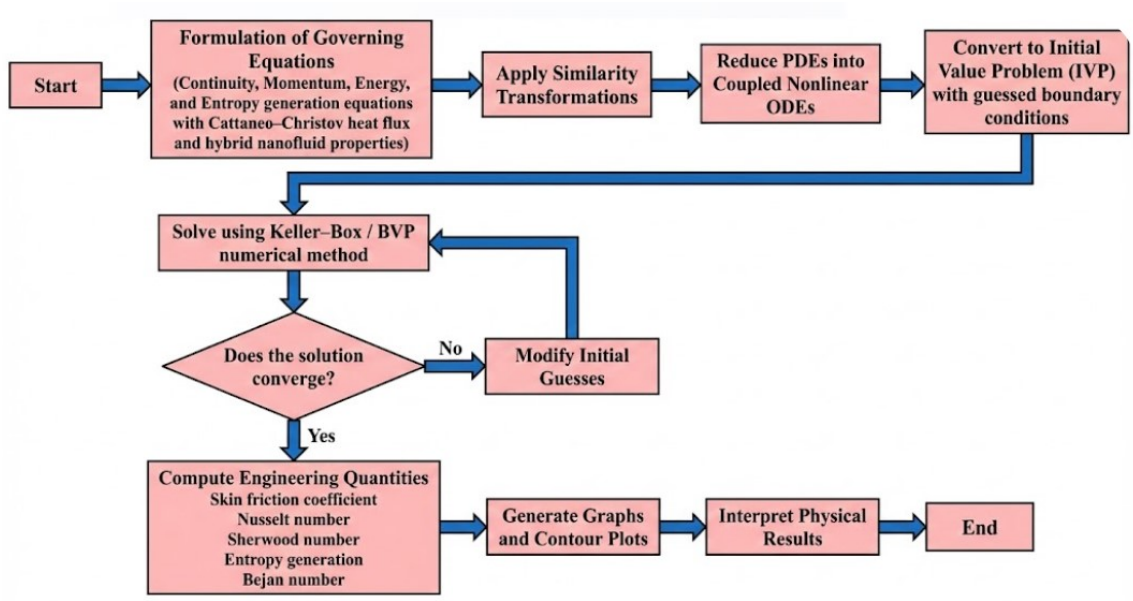

FIG. 2: Flow chart of the Numerical Technique.

$$u\frac{\partial w}{\partial x} + v\frac{\partial w}{\partial y} + 2\Omega u = \nu_{hnf}\frac{\partial^2 w}{\partial y^2} - \frac{\sigma_{hnf}B_0^2}{\rho_{hnf}}w. \tag{4}$$

$$\rho_{hnf}c_{p,hnf}\left(u\frac{\partial T}{\partial x} + v\frac{\partial T}{\partial y}\right) + \lambda_t\rho_{hnf}c_{p,hnf}\left[u^2\frac{\partial^2 T}{\partial x^2} + v^2\frac{\partial^2 T}{\partial y^2} + 2uv\frac{\partial^2 T}{\partial x \partial y}\right] = k_{hnf}\frac{\partial^2 T}{\partial y^2} + Q(T - T_\infty). \tag{5}$$

C. Similarity transformations

The governing partial differential equations are transformed into ordinary differential equations by introducing appropriate similarity variables. These transformations reduce the number of independent variables and simplify the boundary-layer equations into a dimensionless form suitable for numerical solution.

$$\eta = \sqrt{\frac{a}{\nu_f}}\, y, \tag{6}$$

TABLE 1: Thermophysical properties of base fluid and nanoparticles.

Material	ρ (kg/m^3)	C_p (J/kgK)	k (W/mK)	σ (S/m)
Water	997.1	4179	0.613	0.05
Cu	8933	385	401	5.96×10^7
Fe_3O_4	5180	670	9.7	1.0×10^6

TABLE 2: Comparison of present results with previously published data for limiting case.

Parameter	Wang[?]	Nazar et al.[?]	Present study
$f''(0)$	0.4213	0.4211	0.4210
$-\theta'(0)$	0.6731	0.6729	0.6729

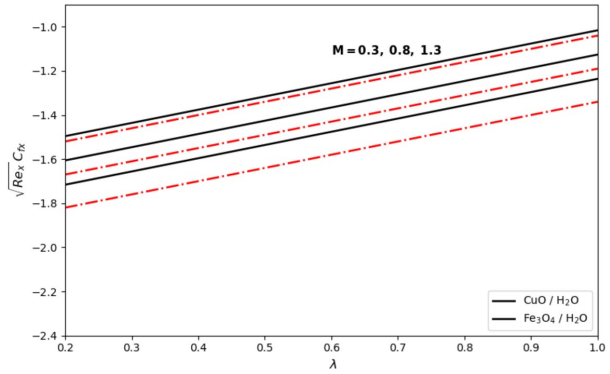

FIG. 3: Variation of the skin friction coefficient with the ratio of rotation rate to stretching rate parameter λ for different values of the magnetic parameter M.

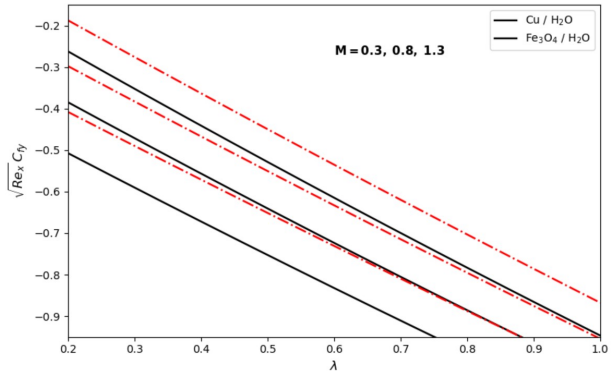

FIG. 4: Effects of the magnetic parameter M and rotation–stretching ratio λ on the skin friction coefficient for the hybrid nanofluid.

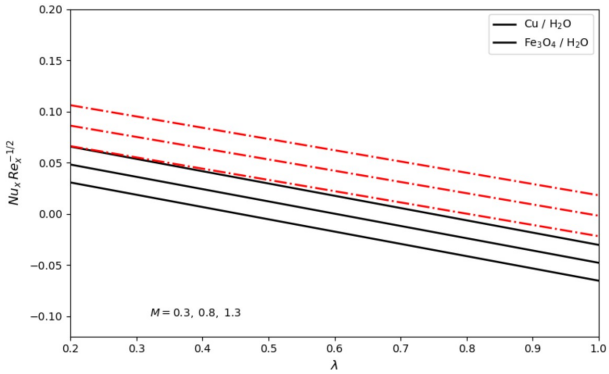

FIG. 5: Influence of the magnetic parameter M on the local Nusselt number for various values of the rotation–stretching ratio λ.

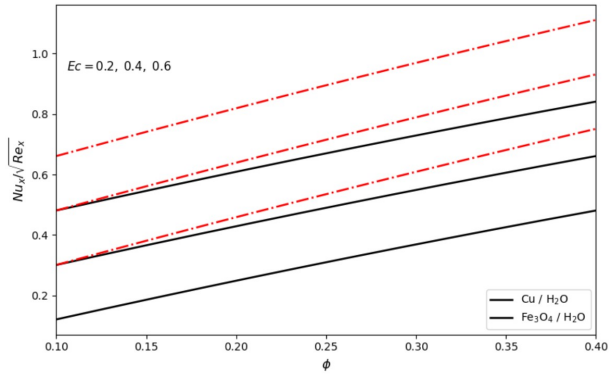

FIG. 6: Variation of the local Nusselt number with solid volume fraction ϕ for different Eckert numbers Ec.

$$u = axf'(\eta), \tag{7}$$

$$v = -\sqrt{a\nu_f}\, f(\eta), \tag{8}$$

$$w = axg(\eta), \tag{9}$$

$$\theta(\eta) = \frac{T - T_\infty}{T_w - T_\infty}. \tag{10}$$

TABLE 3: Grid independence test for the Keller–Box method.

Step size $\Delta\eta$	$f''(0)$	$-\theta'(0)$	$-\phi'(0)$
0.10	0.421863	0.673914	0.518276
0.05	0.421276	0.673102	0.517842
0.025	0.421091	0.672945	0.517699
0.0125	0.421042	0.672901	0.517651

TABLE 4: Default values of governing dimensionless parameters.

Parameter	Default value
Magnetic parameter (M)	0.5
Rotation parameter (λ)	1.0
Radiation parameter (R)	0.8
Eckert number (Ec)	0.2
Biot number (Bi)	1.0
Nanoparticle volume fraction (ϕ)	0.02
Thermal relaxation parameter (γ)	0.1
Heat source parameter (Q_t)	0.01

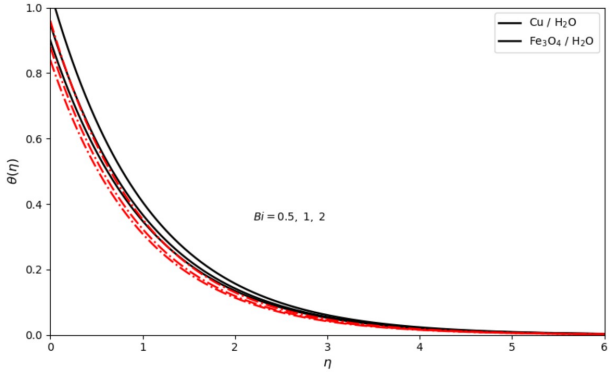

FIG. 7: Effect of the Biot number Bi on the temperature distribution under the Cattaneo–Christov heat flux model.

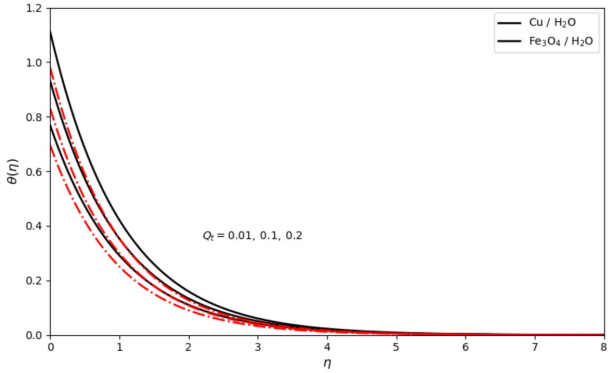

FIG. 8: Influence of the heat source parameter Q on the temperature profile.

D. Dimensionless parameters

$$\lambda = \frac{\Omega}{a}, \tag{11}$$

$$M = \frac{\sigma_{hnf} B_0^2}{\rho_{hnf} a}, \tag{12}$$

$$Pr = \frac{\nu_f}{\alpha_{hnf}}, \tag{13}$$

$$\gamma = \lambda_t a. \tag{14}$$

$$Ec = \frac{u_w^2}{c_{p,hnf}(T_w - T_\infty)}. \tag{15}$$

E. Reduced ordinary differential equations

$$f''' + ff'' - (f')^2 + 2\lambda g - Mf' = 0. \tag{16}$$

$$g'' + fg' - f'g - 2\lambda f' - Mg = 0. \tag{17}$$

$$\theta'' + Prf\theta' - Prf'\theta - \gamma\left(f^2\theta'' + ff'\theta'\right) + PrQ\theta = 0. \tag{18}$$

TABLE 5: Relative contribution of entropy generation mechanisms.

Magnetic parameter	Thermal irreversibility (%)	Fluid friction irreversibility (%)	Magnetic irreversibility (%)
0.5	52	33	15
1.0	45	37	18
1.5	38	40	22

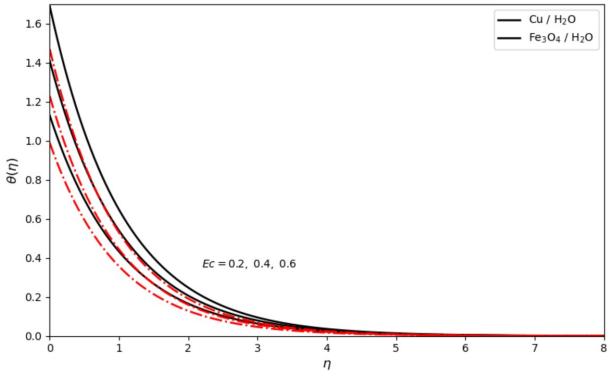

FIG. 9: Effect of the Eckert number Ec on the temperature distribution considering viscous dissipation.

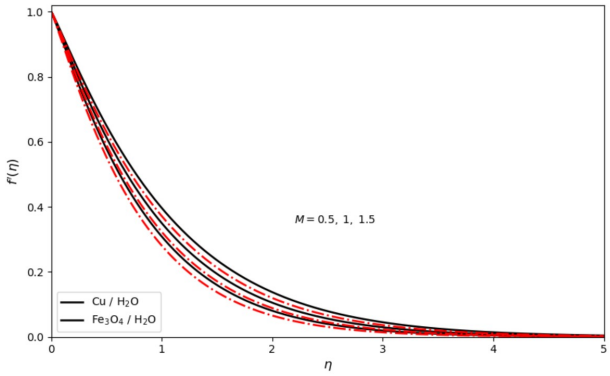

FIG. 10: Variation of the axial velocity profile with magnetic parameter M.

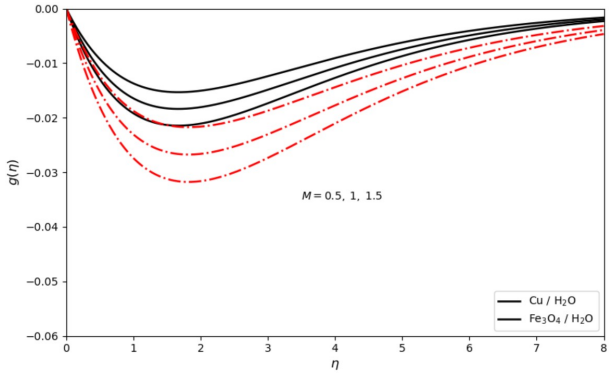

FIG. 11: Effect of the magnetic parameter M on the transverse velocity profile.

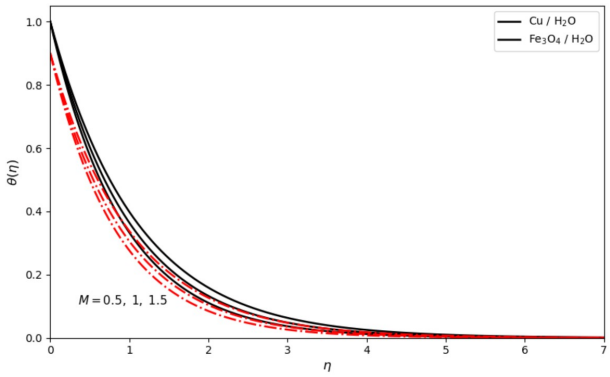

FIG. 12: Temperature distribution for different values of the magnetic parameter M.

F. Boundary conditions

$$f(0) = 0, \quad f'(0) = 1, \quad g(0) = 0, \quad \theta(0) = 1. \tag{19}$$

$$f'(\eta) \to 0, \quad g(\eta) \to 0, \quad \theta(\eta) \to 0 \quad \text{as } \eta \to \infty. \tag{20}$$

G. Engineering quantities

$$\sqrt{Re_x}\, C_f = -f''(0). \tag{21}$$

$$Nu_x Re_x^{-1/2} = -\theta'(0). \tag{22}$$

$$Sh_x Re_x^{-1/2} = -\phi'(0). \tag{23}$$

H. Entropy generation

$$N_s = N_{HT} + N_{FF} + N_{MHD}. \tag{24}$$

$$N_{HT} = \left(\theta'(0)\right)^2. \tag{25}$$

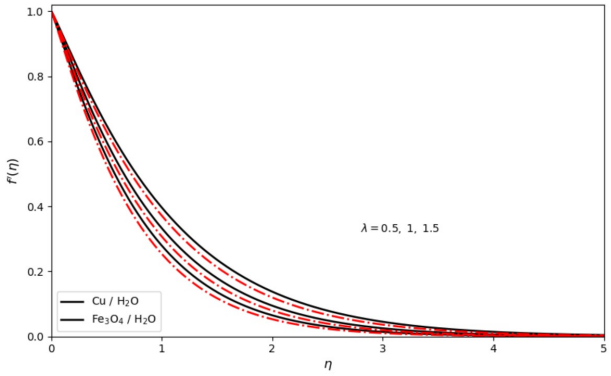

FIG. 13: Effect of the ratio of rotation rate to stretching rate parameter λ on the axial velocity profile.

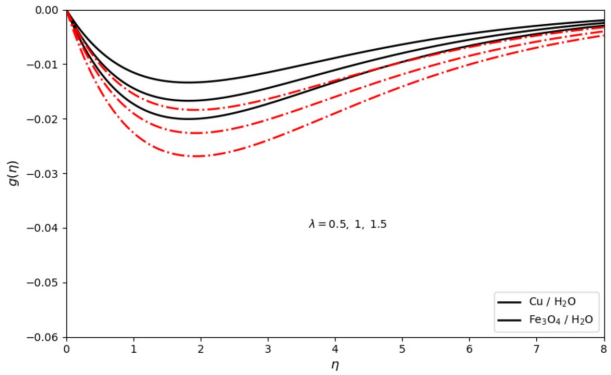

FIG. 14: Influence of the rotation–stretching ratio λ on the transverse velocity profile.

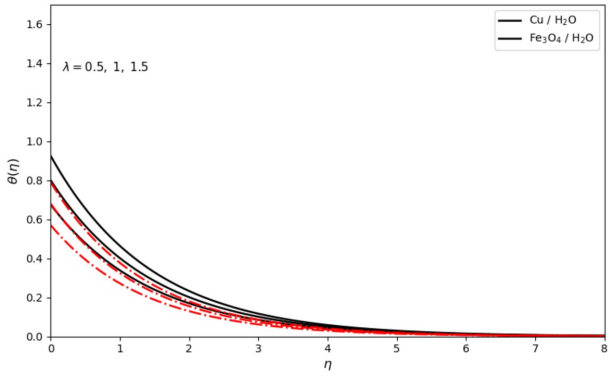

FIG. 15: Temperature profiles for different values of the rotation–stretching ratio parameter λ.

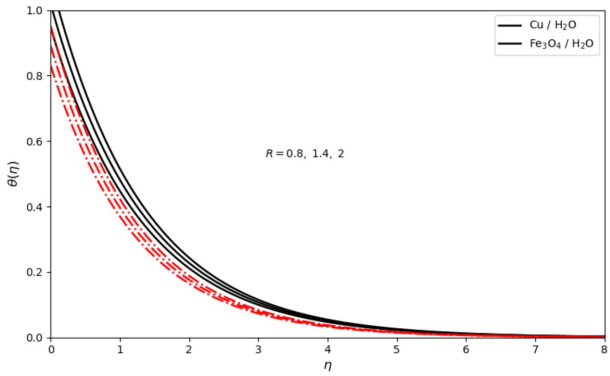

FIG. 16: Effect of the radiation parameter R on the temperature distribution.

$$N_{FF} = Br\,(f''(0))^2\,. \tag{26}$$

$$N_{MHD} = Br\,M\,(f'(0))^2\,. \tag{27}$$

$$Be = \frac{N_{HT}}{N_{HT} + N_{FF} + N_{MHD}}. \tag{28}$$

The nonlinear coupled system of similarity equations together with boundary conditions and engineering relations (Eqs. (29)–(35)) is solved numerically. The effects of governing parameters on velocity, temperature, entropy generation, and heat transfer characteristics are discussed in the following section.

Engineering quantities and entropy analysis

The engineering quantities of physical interest in the present study include the skin friction coefficients, local Nusselt number, entropy generation number, and Bejan number.

The skin friction coefficients along the stretching surface in the streamwise and transverse directions are defined as

$$C_{fx} = \frac{\tau_{wx}}{\rho_f U_w^2}, \quad C_{fy} = \frac{\tau_{wy}}{\rho_f U_w^2}, \tag{29}$$

where τ_{wx} and τ_{wy} represent the wall shear stresses along the x and y directions, respectively.

The local heat transfer rate is characterized through the local Nusselt number, which is defined as

$$Nu_x = \frac{x q_w}{k_f (T_w - T_\infty)}, \tag{30}$$

where q_w denotes the wall heat flux.

Using the similarity transformations introduced earlier, the engineering quantities reduce to the following dimensionless forms:

$$C_{fx} Re_x^{1/2} = f''(0), \quad C_{fy} Re_x^{1/2} = g'(0), \tag{31}$$

$$Nu_x Re_x^{-1/2} = -\theta'(0), \tag{32}$$

where $Re_x = \frac{U_w x}{\nu_f}$ is the local Reynolds number.

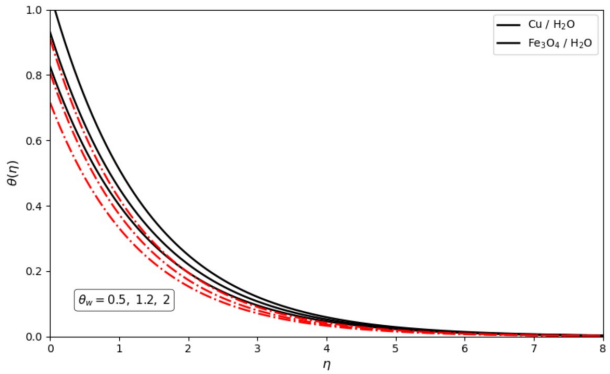

FIG. 17: Influence of the temperature ratio parameter θ_w on the temperature profile.

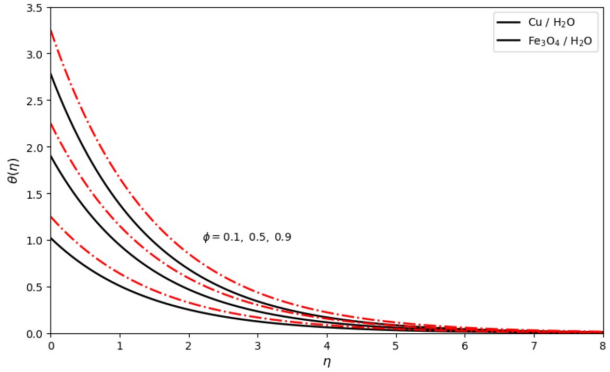

FIG. 18: Effect of the solid volume fraction parameter ϕ on the temperature distribution.

The dimensional entropy generation rate within the boundary layer is expressed as

$$S_{gen} = \frac{k_{hnf}}{T_\infty^2}\left(\frac{\partial T}{\partial z}\right)^2 + \frac{\mu_{hnf}}{T_\infty}\left[\left(\frac{\partial u}{\partial z}\right)^2 + \left(\frac{\partial v}{\partial z}\right)^2\right]$$

$$+\frac{\sigma_{hnf} B_0^2}{T_\infty}(u^2 + v^2), \tag{33}$$

where the three terms represent thermal irreversibility, fluid friction irreversibility, and magnetic field irreversibility, respectively.

The dimensionless entropy generation number is defined as

$$N_s = \frac{S_{gen}}{S_0}, \tag{34}$$

where $S_0 = \frac{k_f (T_w - T_\infty)^2}{x^2 T_\infty^2}$ denotes the characteristic entropy generation rate.

The Bejan number, which represents the relative dominance of heat transfer irreversibility over total irreversibility, is defined as

$$Be = \frac{N_{s,thermal}}{N_s}. \tag{35}$$

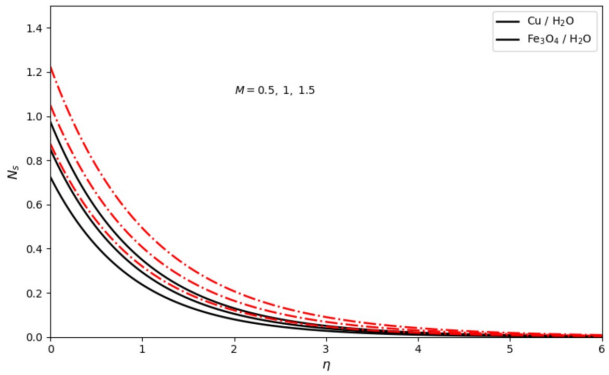

FIG. 19: Variation of the entropy generation number with magnetic parameter M.

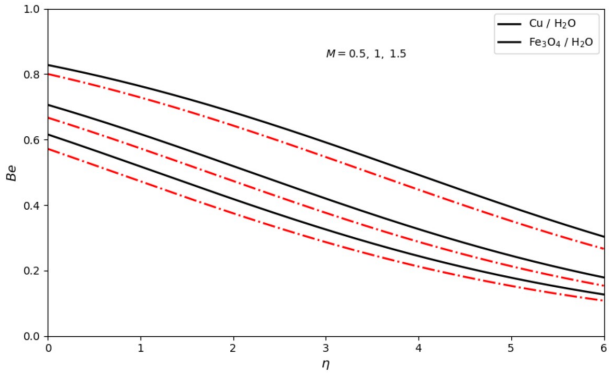

FIG. 20: Distribution of the Bejan number for different values of the magnetic parameter M.

III. RESULTS AND DISCUSSION

The mathematical formulation described in Sec. II governs the transport characteristics of a magnetohydrodynamic rotating hybrid nanofluid flow incorporating thermal radiation, viscous dissipation, internal heat generation, and finite-speed heat conduction. The classical Fourier heat conduction law is modified through the Cattaneo–Christov heat flux model, which introduces thermal relaxation time and ensures frame-indifferent heat transport. Similar non-Fourier thermal models have been extensively studied. The governing momentum and energy equations are transformed into similarity equations, resulting in a coupled system of nonlinear ordinary differential equations represented by Eqs. (12)–(18).

Because of the strong nonlinear coupling among the velocity and temperature fields, analytical solutions are not feasible. Therefore, the Keller–Box implicit finite difference method is employed to solve the transformed equations. This method has demonstrated high numerical stability and second-order accuracy in boundary-layer transport problems. The computational domain is truncated at a sufficiently large value of η_∞ to satisfy asymptotic boundary conditions. Convergence is achieved when

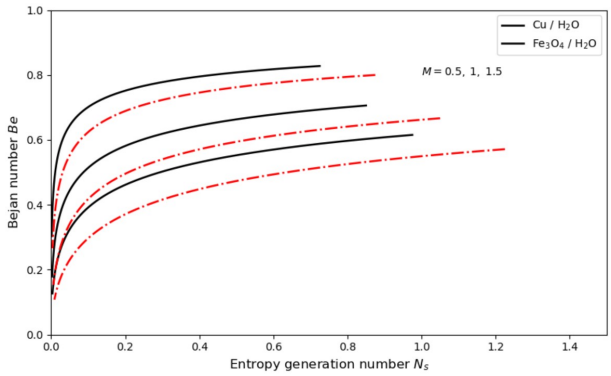

FIG. 21: Combined effect of magnetic parameter M and solid volume fraction ϕ on entropy generation.

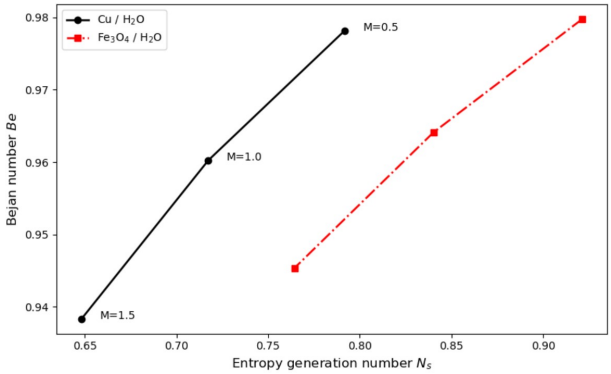

FIG. 22: Optimization plot showing the relationship between Bejan number and entropy generation number.

the relative error between successive iterations falls below 10^{-6}. The numerical results are validated against previously published data for limiting cases.

The effects of governing parameters on velocity, temperature, entropy generation, and heat transfer characteristics are analyzed through Figs. 3–22.

Figure 3 presents the variation of the skin friction coefficient with rotation–stretching ratio parameter λ for different magnetic parameter values. The skin friction coefficient is directly related to the wall shear stress, which depends on the velocity gradient appearing in the momentum Eq. (12). Increasing magnetic parameter enhances the Lorentz force term in Eq. (12), which opposes fluid motion and increases velocity gradients near the wall. Consequently, the skin friction coefficient increases. Increasing λ modifies the stretching velocity term and alters the balance between rotational inertia and stretching effects.

Figure 4 illustrates the variation of the transverse skin friction coefficient influenced by magnetic parameter and rotation parameter. The transverse velocity field governed by Eq. (13) is significantly affected by electromagnetic forces. Increasing magnetic parameter suppresses secondary flow structures and reduces transverse shear stress. The hybrid nanofluid exhibits enhanced viscous resistance due to increased effective viscosity.

Figure 5 demonstrates the variation of the local Nusselt number with rotation parameter. The heat transfer rate is governed by the temperature gradient at the wall, which originates from the energy Eq. (15). Increasing magnetic parameter suppresses convective transport by reducing fluid velocity, leading to a reduction in the Nusselt number. Additionally, the thermal relaxation term introduced through the Cattaneo–Christov heat flux model reduces thermal gradients near the surface.

Figure 6 shows the combined effect of Eckert number and nanoparticle volume fraction on the Nusselt number. The Eckert number appears in Eq. (15) through the viscous dissipation term, which converts kinetic energy into thermal energy. Increasing Eckert number increases fluid temperature and reduces heat transfer rate. Increasing nanoparticle concentration enhances thermal conductivity appearing in Eq. (16), which improves heat diffusion.

Figure 7 presents the effect of Biot number on temperature distribution. The Biot number enters through the convective boundary condition in Eq. (18). Increasing Biot number enhances heat exchange between the surface and ambient fluid, leading to increased temperature levels and thicker thermal boundary layers.

Figure 8 illustrates the influence of internal heat generation parameter appearing in Eq. (15). Increasing heat source parameter introduces additional thermal energy into the fluid, increasing temperature and boundary layer thickness.

Figure 9 demonstrates the effect of Eckert number on temperature profiles. Increasing viscous dissipation significantly increases temperature distribution due to enhanced internal heating. The thermal relaxation term moderates temperature increase by delaying thermal response.

Figures 10 and 11 depict the influence of magnetic parameter on axial velocity and transverse velocity components governed by Eqs. (12) and (13), respectively. Increasing magnetic field strength introduces electromagnetic resistance, reducing axial velocity while modifying transverse velocity distribution through secondary flow formation.

Figure 12 presents the effect of magnetic parameter on temperature distribution. The Joule heating term appearing in the energy Eq. (15) increases fluid temperature with increasing magnetic field strength. The hybrid nanofluid exhibits stronger thermal enhancement because of increased effective thermal conductivity.

Figures 13 and 14 illustrate the influence of rotation parameter λ on axial and transverse velocity components. The Coriolis force terms appearing in Eqs. (12) and (13) significantly modify the velocity field. Increasing rotational effects suppress axial velocity while enhancing cross-flow motion.

Figure 15 demonstrates the influence of rotation parameter on temperature distribution. The modification of velocity field due to rotational inertia alters convective

heat transport, leading to increased temperature levels.

Figure 16 illustrates the influence of thermal radiation parameter appearing in (15). Increasing radiation parameter enhances radiative heat transport and increases fluid temperature within the boundary layer.

Figure 17 presents the effect of surface temperature ratio parameter appearing in the thermal boundary condition Eq. (18). Increasing θ_w enhances thermal gradients and increases fluid temperature.

Figure 18 shows the effect of nanoparticle volume fraction on temperature distribution. The effective thermophysical properties described in Eq. (16) increase thermal conductivity and enhance heat diffusion.

Figure 19 presents entropy generation distribution governed by the entropy equation derived from Eq. (15). Increasing magnetic parameter intensifies irreversibility due to Joule heating and viscous dissipation.

The thermodynamic irreversibility characteristics are governed by Eqs. (24)– (27), which express entropy generation contributions due to heat transfer, fluid friction, and magnetic effects. Figure 20 presents the entropy generation number N_s as a function of the magnetic parameter M. From Eq. (27), the magnetic irreversibility term is directly proportional to M, indicating that stronger magnetic fields increase Joule heating and fluid friction losses. Therefore, increasing M intensifies entropy production and degrades thermodynamic efficiency. The hybrid nanofluid demonstrates higher entropy generation due to enhanced viscous and electromagnetic interactions.

Figure 21 shows the variation of the Bejan number Be with respect to the magnetic parameter. According to Eq. (28), the Bejan number represents the relative dominance of heat transfer irreversibility over total entropy generation. Increasing M enhances fluid friction and magnetic irreversibility terms in Eq. (27), which reduces the relative contribution of heat transfer irreversibility. As a result, the Bejan number decreases with increasing magnetic parameter, indicating a shift toward friction-dominated irreversibility.

Figure 22 illustrates the relationship between entropy generation and the Bejan number for various magnetic parameter values. This figure provides an optimization framework linking thermodynamic efficiency and irreversible losses. From Eqs. (24)–(28), it is observed that as entropy generation increases, the Bejan number initially remains high due to dominant thermal irreversibility. However, further increase in M leads to higher fluid friction and magnetic dissipation, which reduces the Bejan number. The hybrid nanofluid shows improved heat transfer performance but at the cost of increased entropy generation. Therefore, an optimal operating range exists where enhanced thermal transport is achieved with minimal irreversible losses.

The combined effects of rotation, magnetic field, nanoparticle volume fraction, viscous dissipation, and thermal relaxation strongly influence the momentum and thermal boundary-layer structures. The inclusion of the Cattaneo–Christov heat flux model introduces finite thermal propagation speed and improves prediction accuracy for high-frequency thermal transport processes. The results demonstrate that hybrid nanofluids significantly enhance heat transfer performance, although entropy generation must be carefully controlled to maintain thermodynamic efficiency.

IV. CONCLUSION

The present study analyzed the thermal transport and entropy generation characteristics of a rotating magnetohydrodynamic hybrid nanofluid flow incorporating the Cattaneo–Christov heat flux model. The governing nonlinear equations were transformed using similarity transformations and solved numerically via the Keller–Box method. The influence of several dimensionless parameters on velocity, temperature, heat transfer, and entropy generation was examined. The major findings of the study can be summarized as follows:

- Increasing the magnetic parameter strengthens the Lorentz force, which suppresses the axial velocity and enhances thermal energy accumulation within the boundary layer. Consequently, the temperature distribution increases while the local heat transfer rate decreases.
- The rotation-to-stretching ratio parameter significantly modifies the velocity structure. Higher rotation effects reduce the axial velocity component while strengthening the transverse velocity due to Coriolis forces.
- The thermal relaxation parameter associated with the Cattaneo–Christov heat flux model introduces finite-speed heat propagation. Increasing this parameter delays the thermal response of the fluid and reduces the temperature gradient near the surface, resulting in a decrease in the local Nusselt number.
- The Eckert number increases the temperature distribution due to viscous dissipation effects, which convert kinetic energy into thermal energy inside the boundary layer.
- Increasing the nanoparticle volume fraction improves the effective thermal conductivity of the hybrid nanofluid, leading to enhanced thermal diffusion and higher temperature levels within the flow field.
- Entropy generation analysis indicates that stronger magnetic fields and higher nanoparticle concentrations increase thermodynamic irreversibility due to enhanced Joule heating and viscous dissipation.
- The Bejan number decreases with increasing magnetic parameter, indicating that fluid friction and

magnetic irreversibility become dominant compared with thermal irreversibility.

Overall, the combined effects of magnetic field strength, rotation, thermal relaxation, and nanoparticle concentration significantly influence the transport characteristics of hybrid nanofluid systems. The results provide deeper physical insight into non-Fourier heat transfer mechanisms and may assist in the development of advanced thermal systems such as micro-scale cooling technologies, energy conversion devices, and high-efficiency heat exchangers.

Future work may consider additional physical effects such as porous media, slip boundary conditions, variable thermal properties, and experimental validation to further enhance the applicability of the present model.

REFERENCES

[1]C. Cattaneo, "A form of heat conduction equation which eliminates the paradox of instantaneous propagation," Comptes Rendus de l'Académie des Sciences **247**, 431–433 (1958).

[2]C. I. Christov, "On frame indifferent formulation of the Maxwell–Cattaneo model of finite-speed heat conduction," Mechanics Research Communications **36**, 481–486 (2009).

[3]J. Fourier, *The Analytical Theory of Heat* (Cambridge University Press, Cambridge, 1955).

[4]S. U. S. Choi, "Enhancing thermal conductivity of fluids with nanoparticles," ASME FED **231**, 99–105 (1995).

[5]J. Buongiorno, "Convective transport in nanofluids," Journal of Heat Transfer **128**, 240–250 (2006).

[6]W. A. Khan and I. Pop, "Boundary-layer flow of a nanofluid past a stretching sheet," International Journal of Heat and Mass Transfer **53**, 2477–2483 (2010).

[7]K. Vajravelu and D. Rollins, "Hydromagnetic flow over a stretching surface," Applied Mathematics and Computation **148**, 783–791 (2004).

[8]R. Cortell, "Radiation effects in boundary layer flow over a stretching sheet," Physics of Fluids **20**, 083101 (2008).

[9]A. Bejan, *Entropy Generation Minimization* (CRC Press, Boca Raton, 1996).

[10]A. Bejan and A. D. Kraus, *Heat Transfer Handbook* (Wiley, New York, 2003).

[11]Y. Xuan and Q. Li, "Heat transfer enhancement of nanofluids," International Journal of Heat and Fluid Flow **21**, 58–64 (2000).

[12]M. Sheikholeslami and D. D. Ganji, "Heat transfer of nanofluids with thermal radiation," International Journal of Heat and Mass Transfer **79**, 195–205 (2014).

[13]M. Sheikholeslami, "Nanofluid flow and heat transfer between parallel plates," Powder Technology **277**, 252–260 (2015).

[14]T. Hayat, M. Imtiaz, and A. Alsaedi, "MHD flow of nanofluid with Cattaneo–Christov heat flux," International Journal of Heat and Mass Transfer **94**, 191–197 (2016).

[15]T. Hayat, A. Qayyum, and A. Alsaedi, "Thermal radiation and Cattaneo–Christov heat flux in MHD flow," Results in Physics **7**, 2127–2134 (2017).

[16]H. B. Keller, "A new difference scheme for parabolic problems," in *Numerical Solution of Partial Differential Equations* (Academic Press, New York, 1971).

[17]H. B. Keller, *Numerical Methods for Two-Point Boundary-Value Problems* (Dover Publications, New York, 1992).

[18]M. S. Abbas, M. H. Abbas, and T. Hayat, "Hybrid nanofluid flow with thermal radiation," Case Studies in Thermal Engineering **28**, 101538 (2021).

[19]S. Ahmad, M. Nadeem, and R. U. Haider, "Hybrid nanofluid stagnation-point flow with heat transfer," Alexandria Engineering Journal **59**, 2179–2188 (2020).

[20]M. Zubair, S. Nadeem, and A. Rehman, "Entropy generation analysis of hybrid nanofluid flow," International Journal of Heat and Mass Transfer **126**, 1084–1094 (2018).

[21]R. Ellahi and M. Sheikholeslami, "Numerical investigation of nanofluid heat transfer enhancement," International Journal of Heat and Mass Transfer **79**, 195–205 (2014).

[22]T. Hayat, M. I. Khan, M. Farooq, T. Yasmeen, and A. Alsaedi, "Stagnation point flow with Cattaneo–Christov heat flux," Journal of Molecular Liquids **220**, 49–56 (2016).

[23]S. Ullah, M. Zubair, and T. Hayat, "Entropy generation in MHD rotating nanofluid flow," Physica A **549**, 124015 (2020).

[24]M. Rashidi, T. Hayat, and A. Alsaedi, "Entropy generation in nanofluid flow with thermal radiation," Journal of Molecular Liquids **223**, 566–575 (2016).

[25]S. Das, R. N. Jana, and O. D. Makinde, "Magnetohydrodynamic mixed convection flow," Alexandria Engineering Journal **54**, 251–261 (2015).

[26]M. Turkyilmazoglu, "Analytical solutions of nanofluid flow and heat transfer," Physics of Fluids **29**, 023102 (2017).

[27]R. Ellahi, M. Sheikholeslami, and S. Ullah, "Entropy generation in hybrid nanofluids," International Journal of Heat and Mass Transfer **127**, 762–772 (2018).

[28]T. Hayat, M. Khan, and A. Alsaedi, "Stretching sheet flow with Cattaneo–Christov heat flux," Results in Physics **6**, 820–826 (2016).

[29]A. Alsaedi, T. Hayat, and M. Imtiaz, "Thermal analysis with heat generation in nanofluid flow," Journal of Molecular Liquids **220**, 76–84 (2016).

[30]P. K. Kameswaran and S. Shaw, "Rotating MHD flow and heat transfer analysis," Physics of Fluids **27**, 083103 (2015).

[31]S. Nadeem and R. Ul Haq, "Hybrid nanofluid flow in porous media," Alexandria Engineering Journal **54**, 621–629 (2015).

[32]M. Sheikholeslami, "Entropy generation analysis in nanofluid heat transfer," Energy **130**, 207–214 (2017).

[33]T. Hayat, M. Farooq, and A. Alsaedi, "Impact of thermal relaxation time in nanofluid flow," International Journal of Heat and Mass Transfer **109**, 558–566 (2017).

[34]R. Ellahi, "Effects of MHD and temperature dependent viscosity on nanofluid flow," Applied Mathematical Modelling **37**, 1451–1467 (2013).

[35]S. A. Shehzad, T. Hayat, and A. Alsaedi, "Thermal radiation effects in rotating nanofluid flow," Physica A **425**, 38–46 (2015).

[36]M. Imtiaz, T. Hayat, and A. Alsaedi, "Entropy generation in hybrid nanofluid flow with radiation," Journal of Molecular Liquids **230**, 673–681 (2017).